Multiband polarization insensitive and tunable terahertz metamaterial perfect absorber based on the heterogeneous structure of graphene

Amirhossein Norouzi-Razani[1] · Pejman Rezaei[1]

Abstract

In this paper, we present and investigate a multi-band metamaterial perfect absorber based on the heterogeneous structure of graphene with Cu and SiO_2 substrates. The top layer of structure consists of one graphene disk at the center and four graphene solid triangle with semicircular cuts on them that surround the central disk. This heterogeneous structure causes us to achieve 99.5%, 99.7%, 94.71% and 97.06% perfect absorptions peaks at 4.24 THz, 5.89 THz, 9.66 THz and 10.62 THz, respectively. The absorption mechanism based on electric fields has been investigated. We can shift the wavelength of absorption peaks to our required wavelength by changing the Fermi level (μ_c) of graphene. Two absorption peaks of this absorber remain unchanged in different light incident angles. In addition, very important point about this structure is that it is not sensitive to polarization and this feature makes the proposed absorber very suitable for applications such as imaging, filtering, sensing and detecting applications.

1 Introduction

With the increasing development of communication technology and the use of frequency in the terahertz range, the need for tools and equipment in this frequency range is inevitable. This need drew the attention of all terahertz range researchers to metamaterials.

A metamaterial is any material engineered to have a property that is not found in naturally occurring materials (Kshetrimayum 2004). Metamaterials have special properties such as negative refraction (Valentine et al. 2008; Veselago 1968), cloak (Shin 2012; Cai 2007) superlunary (Smith et al. 2004; Pendry 2000) and backward wave (Song et al. 2012; Simovski et al. 2003), and for this reason, they have been highly regarded by researchers in the field of electromagnetism. In addition, metamaterials are very useful in the construction

✉ Pejman Rezaei
   prezaei@semnan.ac.ir

[1] Electrical and Computer Engineering Faculty, Semnan University, Semnan, Iran

and design of solar energy absorbers (Zhao et al. 2022; Zhao et al. 2021), switchable tera-hertz devices (Zheng et al. 2022), refractive index sensors (Wu et al. 2021), waveguide-Cavities (Deng et al. 2018, 2015), and etc.

One of the most important and practical metamaterials is graphene. Graphene is a metamaterial made of graphite, and graphite itself is made up of layers of carbon atoms arranged hexagons. There is a Van der Waals bond (a rather weak chemical bond) between these layers. By breaking these bonds according to Fig. 1, we can reach the graphene meta-material, which is a single layer of carbon atoms, and because of this, it is called a two-dimensional metamaterial (Katsnelson 2007).

Graphene has received a great deal of attention in the construction of antennas and alter-nating structures, including absorbers, electromagnetic shields, and electromagnetic sen-sors, due to its small size, two-dimensionality, high conductivity and its adjustable conduc-tivity (Ghods and Rezaei 2018a, b; Pop 2012). In recent decades, extensive research and developments have been done in the field of design and improvement of tools and devices that have been made and designed using graphene. Due to the use of graphene in antennas has brought us significant benefit such as extreme miniaturization, monolithic integration with graphene RF Nano- electronics, efficient dynamic tuning, and even transparency and mechanical flexibility (Perruisseau-Carrier 2012), the idea of designing graphene antennas has been a step to ahead.

Since we can change the chemical potential of graphene by external bias voltage or chemical doping, graphene is an adjustable metamaterial (Zamzam et al. 2021). We used this graphene capability to design the antennas with performance in far-field and terahertz range central frequency due to control its polarization just by changing the Fermi energy level of the graphene (Jafari-Chashmi et al. 2020a, b; Jafari-Chashmi et al. 2020a, b; Kiani et al. 2021a, b; Jafari-Chashmi et al. 2019).

Another application of graphene is the design and construction of absorbers that operate in the microwave (Kiani et al. 2021a, b; Ghods and Rezaei 2018a, b) and terahertz (Gong et al. 2021; Chahkoutahi et al. 2021) range. Tunable absorbers can be obtained by changing the Fermi level of graphene (μ_c) (Xiao et al. 2018). Electromagnetic absorbers are specifi-cally selected or designed materials that can inhibit the reflection or transmission of elec-tromagnetic radiation. Features that are important in absorbers are full absorption (close to 100% adsorption), insensitivity to polarization of radiation and light incident angle.

Absorbers that use metamaterials in their design and have absorption close to 100% are called metamaterial perfect absorbers (MPA) (Ni et al. 2017; Zamzam and Rezaei 2021; Ke et al. 2020; Yao et al. 2016). There are two types of absorbers: resonant (nar-row band) absorbers (Fu et al. 2021; Li et al. 2017; Barzegar-Parizi 2019) and wide-band absorbers (Deljoo et al. 2021; Elrashidi and Tharwat 2021; Bağmancı et al. 2017).
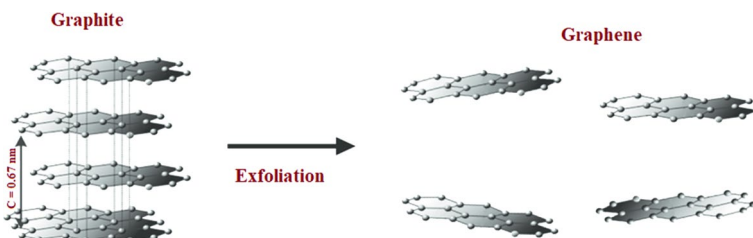
Fig. 1 Exfoliation of graphite to create graphene

Terahertz band absorbers have many applications such as sensing, imaging, modulating, detection, filtering, etc. (Bai et al. 2021; Song et al. 2018; Meng et al. 2018).

The mechanism of absorption of multilayer absorbers is such that the underlying conductive layer does not allow radiation to pass through the structure. In addition, the intermediate dielectric layer and the metamaterial placed on the dielectric must also be designed so that the waves reflected from inside the structure have a phase difference aiming to neutralize each other, in order to the structure reach to the perfect absorption.

One of the characteristics that makes the absorber structure unique for different applications is the insensitivity of the structure to polarization (Shalini 2021; Bendelala et al. 2018) and different light incident angles (Pan et al. 2021).

In this paper, we present a novel design of a multi-band perfect metamaterial absorber that has one graphene disk at the center and four graphene solid triangles with semicircular cuts on them that surround the central disk. This new design is based on tuning and optimization of various design parameters such as structural dimensions, dielectric constant, the conductivity of the conductive layer, chemical potential, and relaxation time of graphene. The dielectric of the middle layer and the conductive of underlying layer of the structure are SiO_2 and Cu, respectively. One of the advantages of this structure is in its construction, because in this structure, copper conductor is used in the lower layer to prevent radiation transmission, which is more economical than structures in which gold is used in the lower layer (Feng et al. 2020; Yi et al. 2019; Wu 2019; Zhang et al. 2018). The proposed absorber is a resonant absorber that has four perfect absorption peaks, which are 99.5%, 99.7%, 94.71% and 97.06% at frequencies of 4.24 THz, 5.89 THz, 9.66 THz, and 10.62 THz, respectively.

2 Graphene conductivity and theoretical discussion

Graphene is a two-dimensional metamaterial that has semi-metallic properties in the terahertz range. Graphene conductivity can be calculated using Kubo formulas (Eqs. (1–3)) (Zamzam et al. 2021). The conductivity of graphene according to Eq. 1 consists of two parts, inter-band and intra-band. The inter-band part can be calculated by Eq. (2) and the intra-band part can be calculated by Eq. (3).

$$\sigma\big(\omega, \tau, \mu_C, T\big) = \sigma_{\text{inter}}\big(\omega, \tau, \mu_C, T\big) + \sigma_{\text{intra}}\big(\omega, \tau, \mu_C, T\big) \tag{1}$$

$$\sigma_{\text{inter}}\big(\omega, \tau, \mu_C, T\big) = -j\frac{e^2}{4\pi\hbar} ln\left(\frac{2\mu_C + \big(\omega - j\tau^{-1}\big)\hbar}{2\mu_C - \big(\omega - j\tau^{-1}\big)\hbar}\right) \tag{2}$$

$$\sigma_{\text{intra}}\big(\omega, \tau, \mu_C, T\big) = -j\frac{e^2 k_B T}{\pi\hbar^2\big(\omega - j\tau^{-1}\big)}\left[\frac{\mu_C}{k_B T} + 2ln\left(\exp\left(-\frac{\mu_C}{k_B T}\right) + 1\right)\right] \tag{3}$$

where ω, τ and μ_c represent the angular frequency, the relaxation time and chemical potential of graphene, respectively, T, e, k_B, and $\hbar$ show the ambient temperature (in this paper T = 300 K), the electron charge (here e = 1.6×10^9 c), the Boltzmann's constant, and the reduced Plank's constant, respectively.

According to the Pauli exclusion principle and since we have $\mu c \gg k_B T$ in the terahertz and infrared bands, the inter-band part of graphene conductivity can be ignored in Eq. (1) and this equation can be simplified to the following equation (like a Drude model):

$$\sigma(\omega, \tau, \mu_C) = \frac{je^2 \mu_C}{\pi \hbar^2 (\omega + j\tau^{-1})} \tag{4}$$

The relaxation time of graphene in Eq. (4) is $\tau = v\mu_C / eV_F^2$, Where v and V_F represents the electron mobility and Fermi velocity (approximately 10^6 m/s).

Electromagnetic absorbers are mainly composed of three layers: two perfect conductor layers and a dielectric layer, which is located between these two conductive layers and is also known as the spacer layer. The general formula for calculating the absorption of electromagnetic absorbers can be written as follows:

$$A = 1 - T - R \tag{5}$$

where A is the absorption coefficient of the structure, T is the transmission coefficient of electromagnetic waves from the structure and R shows the reflection coefficient of electromagnetic waves from the absorber. In many structures, such as the proposed structure, metamaterials such as graphene can be used in the top layer instead of the perfect conductors. In addition, it should be noted that the thickness of the bottom conductor layer should be greater than the penetration depth of terahertz waves in order to reduce the terahertz wave transmission coefficient from the structure to zero (T=0) and simplify Eq. (5) to the following equation:

$$A = 1 - R \tag{6}$$

Figure 2 shows the equivalent circuit model of the proposed absorber. A short transmission line with $Z_{Cu}=0$ impedance is used to model the conductor of the substrate, which is made of copper in the proposed structure. SiO_2 dielectric modeling is also performed using a transmission line with impedance of Z_{TL} and electric length of $E_{TL} = 2 \times \beta_{TL} \times T_S$. For graphene modeling, an R, L, and C branch is used. If the number of graphene layers in the structure of an absorber is more than one, for each additional layer, another R, L, and C branch will be added in parallel to the other branches. Considering the free space impedance equal to $377\,\Omega = 120\,\pi$, the input surface impedances of the presented model in Fig. 2 can be calculated as follows (Norouzi-Razani and Rezaei 2022):

Fig. 2 The equivalent circuit model of the proposed perfect absorber
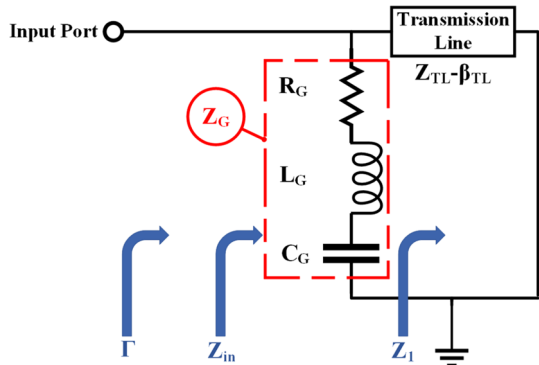
$$Z_1 = jZ_{TL}\tan\left(\beta_{TL}T_s\right) \tag{7}$$

$$\beta_{TL} = 2\pi f \sqrt{\varepsilon_0 \varepsilon_r \mu_0} \tag{8}$$

$$Z_{TL} = \sqrt{\mu_0/\varepsilon_0 \varepsilon_r} \tag{9}$$

$$Z_G = R + jX_G = R + j\left(2\pi fL - \frac{1}{2\pi fC}\right) \tag{10}$$

$$Z_{in} = \frac{Z_1 . Z_g}{Z_1 + Z_g} \tag{11}$$

where β_{TL} and ε_r show the wavenumber and relative permittivity of the dielectric, respectively; in addition, ε_0 and μ_0 represent the relative permittivity and magnetic permeability of the free space, respectively. The values of R, L, and C can be calculated using the following equations (Rezagholizadeh et al. 2020):

$$R = \frac{KL^2}{\pi S^2}\frac{\hbar^2}{e^3\mu_C\tau} \qquad L = \frac{KL^2}{\pi S^2}\frac{\hbar^2}{e^3\mu_C} \qquad C = \frac{\pi^2 S^2}{L^2 k}\frac{\varepsilon}{q_1} \tag{12}$$

where ε, q_1, L, and $\hbar$ are the permittivity of the dielectric, the first eigenvalue of the equation governing the surface current on the graphene layer, the period of unit cells, and the reduced Plank's constant, respectively. K and S are the integral of the internal multiplication of an eigenfunction with the corresponding eigenvalue in the convolution of this eigenfunction and the integral of the eigenfunctions of the equation governing the graphene surface current, respectively, and can be calculated by referring to Ref. (Barzegar-Parizi et al. 2015). According to these equations, the reflection efficiency (Γ) can be calculated using the following equation:

$$\Gamma = \frac{Re\left(Z_{in}\right) - Z_0}{Re\left(Z_{in}\right) + Z_0} \tag{13}$$

On the other hand, since $R = \Gamma^2$, Eq. (1) can also be defined as follows:

$$A = 1 - \Gamma^2 \tag{14}$$

3 Structure and design

As shown in Fig. 3a, we present a three-layer absorber. The bottom layer of the absorber is a cube with dimensions $L \times L$ ($L = 3$ μm) and a thickness of 0.5 μm. The material of this substrate is copper with conductivity of $\sigma_{Cu} = 5.813 \times 10^7$ S/m (Tahseen and Kishk 2016). This conductor has the task of reducing the radiation transmission from the structure to zero. Our middle layer is a cube with the same dimensions $L \times L$ and a thickness of 4.9 μm.
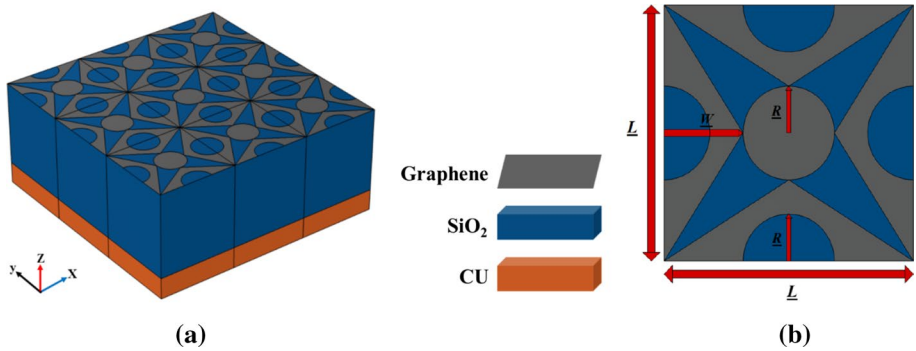
Fig. 3 a Unit cells structure from three-dimensional view. **b** Dimensions of the absorber structure from a two-dimensional view

In addition, its dielectric material is SiO$_2$ with a relative permittivity of $\epsilon_r = 3.9$ (Deng et al. 2014; Chen and Alù 2011).

As mentioned, graphene is a two-dimensional material that is placed on our SiO$_2$ layer. According to Fig. 3b, the central graphene disk has a radius of R = 0.55 μm. The four triangles that surround the central disk are equal in size. The height of each triangle is w = 0.95 μm and the base of each of them is equal to L = 3 μm. We also cut each triangle into a semicircle so that all the semicircles are equal and have a radius R = 0.55 μm.

4 Simulation results

We performed the simulations at room temperature (T = 300 K) using the CST Studio Suite software. As shown in Fig. 4, by setting the parameters of graphene to μ$_c$ = 0.8 eV and τ = 1.6 ps, the structure has four perfect absorption peaks, which are 99.5%, 99.7%, 94.71% and 97.06% at 4.24 THz, 5.89 THz, 9.66 THz and 10.62 THz, respectively.

This structure is tunable; it means that we can shift the frequency of absorption to a required frequency for the intended application or increase and decrease the amount of absorption at the desired frequency by changing Fermi level or relaxation time of graphene. We changed the Fermi level of graphene to different values, and you can see the frequency changes of the absorption peaks in Fig. 5. We also changed the relaxation time of graphene in Fig. 6, where you can see the changes in the absorption peaks of the structure.
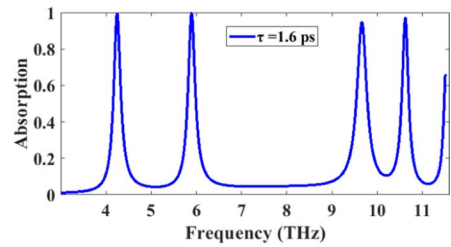
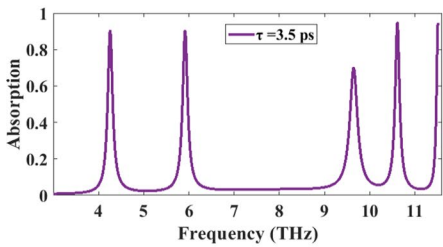**Fig. 4** Absorption spectra of structure with μ$_c$ = 0.8 eV and τ = 1.6 ps
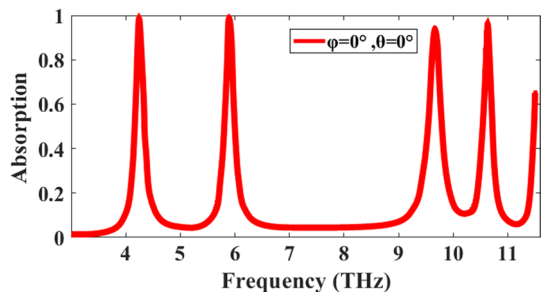
Fig. 5 Absorption spectra of structure for different Fermi level (μ_c) at $\tau = 1.6$ ps
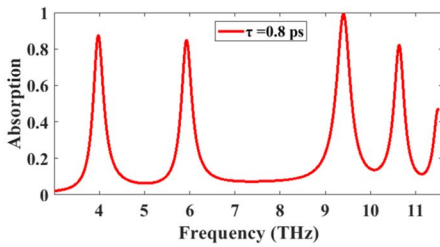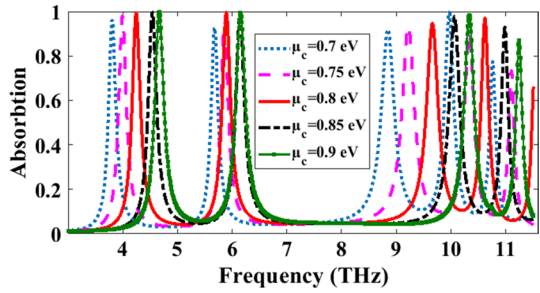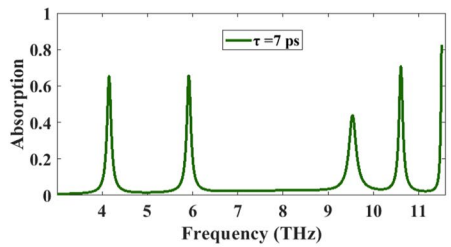
Fig. 6 Absorption spectra of structure at $\mu_c = 0.8$ eV for **a** $\tau = 0.8$ ps, **b** $\tau = 1.6$ ps, **c** $\tau = 3.5$ ps, and **d** $\tau = 7$ ps

Fig. 7 Increasing the number of absorption peaks by setting $\mu_c = 0.5$ eV and $\tau = 3$ ps
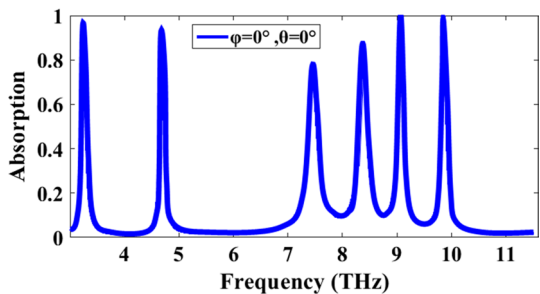
As you can see in Fig. 7, one of the good advantages of this structure is that we can increase the number of absorption peaks by changing the Fermi level of graphene (for example changing it to 0.5 eV) and changing the relaxation time of graphene (for example changing it to 3 ps). By this setting our structure has six absorption peaks, four of those are above 90%, one of those is above 85% and the other one is above 75%. This setting is used
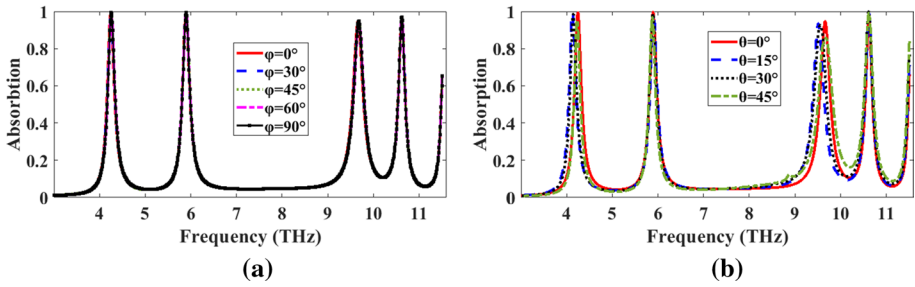
Fig. 8 Absorption spectra of structure for **a** different polarization angles and **b** different light incident angles
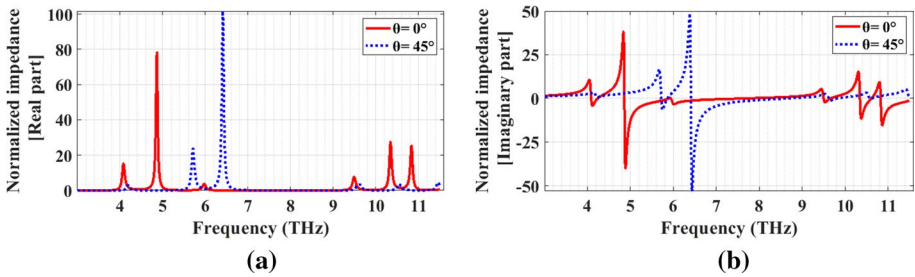
Fig. 9 Normalized impedance of proposed structure **a** real part and **b** imaginary part

for applications where the number of absorption peaks takes precedence over the absorption rate.

One feature that is very important in absorbers is the insensitivity of the structure to polarization. As you can see in Fig. 8a, the absorber presented in this paper is polarization insensitive because the absorption peaks remain unchanged at different angles of polarization. This feature makes the proposed absorber very suitable for applications such as imaging, detecting, filtering, sensing, etc.

As shown in Fig. 8b, it is obtained that the absorption peaks at frequencies 5.89 THz and 10.62 THz with different light incident angles (From 0 to 45 degrees) remain almost unchanged and the absorption peaks at frequencies 4.22 THz and 9.66 THz have a high tolerance (with a little frequency shift) against different light incident angles (From 0 to 45 degrees). Especially at the 10.62 THz peak, the absorption rate increases slightly with increasing light incident angle. In order to investigate the non-change of absorption peaks at frequencies 5.89 THz and 10.62 THz with increasing light incident angle up to 45 degrees, in Fig. 9, the plots of the real part and the imaginary part of the normalized impedance of the proposed structure are presented for the light incident angles of 0 and 45 degrees. As you know, when the real part of the normalized impedance gets closer to 1 and the imaginary part gets closer to 0, the structure gets closer to the impedance matching conditions. Figure 9a and b also show that under a 45-degree light incident angle at absorption peak frequencies, the amount of real parts is close to 1 and the amount of imaginary parts is close to 0 (just same as the 0-degrees light incident angle). Therefore, by increasing the impact angle up to 45 degrees, the structure still has perfect absorption in 4 bands. In addition, the reason for the increase in the absorption rate at the peak of 10.62 THz at the light incident angle of 45-degrees compared to the 0-degrees is that at this frequency, under

an oblique light incident angle, the structure becomes closer to the impedance matching conditions. The frequency shift of the absorption peaks is also due to the parasitic resonance generated at the large light incident angles. All of these make the proposed absorber more widely used in various applications.

5 Discussion and comparison

The absorption mechanism of this absorber is such that the bottom layer of copper does not allow radiation to pass through the structure. In addition, the middle layer of SiO_2 and graphene placed on the layer of SiO_2 is also designed in such a way that the waves reflected from inside the structure have a phase difference and neutralize each other, thus the structure reaches four full absorption peaks.

Plasmons formed at the interface of a metal and dielectric are called surface plasmons. Surface plasmons are excited by visible or ultraviolet photons, a phenomenon called "surface plasmon resonance" (SPR). Surface plasmons are surface-bound plasmons that react strongly with light from paritons. They occur at the interface between a vacuum and a material with a dielectric constant with a small positive real part and a large negative imaginary part. To study surface plasmon, the behavior of metals against light electromagnetic fields must first be studied. The optical response of metals is known by their dielectric function. Plasmon plays an important role in the optical properties of metals, which according to the intended application, we coordinate the frequency of light that we want to reflect with the frequency of plasma to resonate. Nanoparticles have a large number of surface atoms compared to the atoms within their volume. This in itself increases the importance of surface effects compared to volumetric effects. In fact, nanoparticles in response to external fields and forces show effects that depend on the size and shape of the particle and the same ratio to the dielectric constant of the environment and metal, so the size of nanoparticles can be estimated in the diagram of the light spectrum. The dependence of the optical spectrum of large nanoparticles on their size is an external effect that is controlled only by the dimensions of the particle relative to the electromagnetic radiation. Slight changes in the dielectric around the nanoparticle affect the resonance of surface plasmons so that these changes are reflected in the amount of beam scattered, the absorbed beam, or the change in wavelength. When the oscillation frequency of the generated plasmon is equal to the frequency of incident electromagnetic waves, the phenomenon of "local surface plasmon resonance" (LSPR) occurs. By doing this, the electromagnetic field is concentrated in a very small space of about 100 cubic nanometers. Any object that enters this area, called a nano-focus, affects the LSPR. We presented the LSPRs of the proposed structure by calculating electric fields at absorption peak frequencies in Fig. 10.

Figure 10 shows the electric field [real (Ez)] distributions in the normal incidence of TE waves at frequencies of absorption peaks. As you can see in Fig. 10a, the field distribution is mainly concentrated on the lower two corners and along the sides of the triangles located in the x direction. Therefore, we can conclude that the first resonance at frequency of 4.24 THz is due to resonance at these points. Figure 10b shows that the electric field is mainly concentrated on a part of the surface of graphene triangles located in the y direction along the semicircular cuts and the graphene disk, and this concentration extends to the edges of the graphene disk. So the second resonance at the frequency of 5.89 THz is attributed to the resonance of these points. A similar analysis of Fig. 10c shows that the electric field is concentrated on the surface of the graphene triangles located in the x direction and on the inner
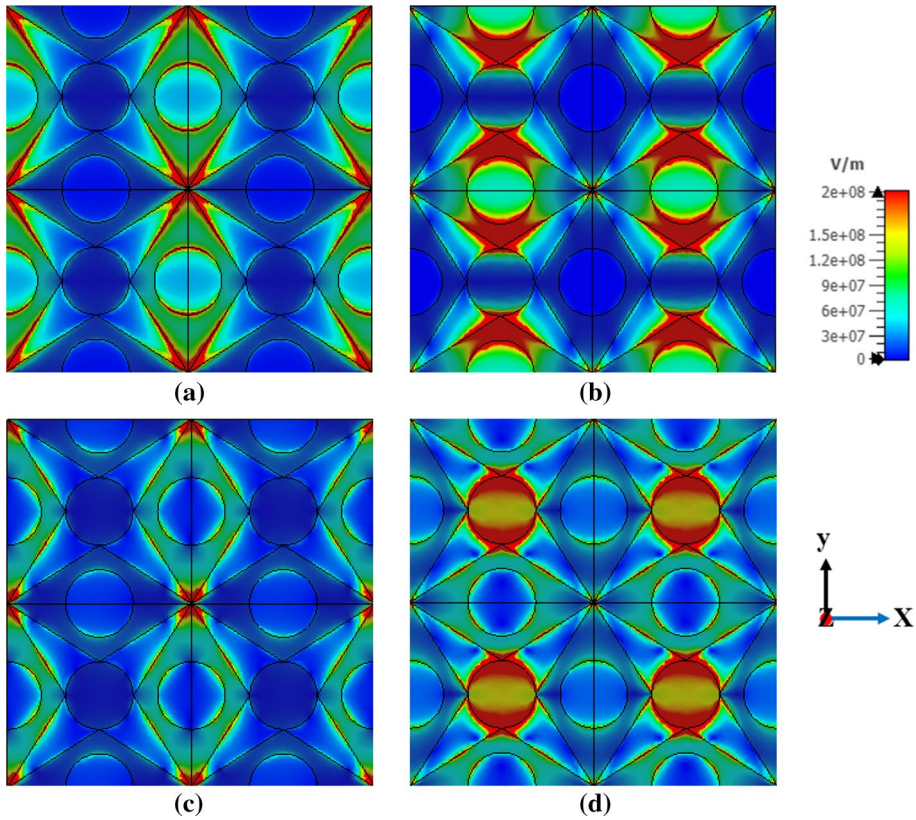
Fig. 10 Electric field [real (Ez)] distributions in the normal incidence of TE waves at frequencies of a 4.24 THz, **b** 5.89 THz, **c** 9.66 THz, and **d** 10.62 THz

edges of the graphene disk. As a result, the third resonance at wavelength of $\lambda = 31,048.9$ nm can be considered due to the graphene resonance at these points. Finally, in Fig. 10d, it is clear that the electric field is concentrated on the intersection of the graphene disk and the graphene triangle located in the y direction, Perimeter of semicircular cuts located in the y direction, the bottom two corners and along the sides of each graphene triangle. Therefore, we can conclude that the fourth resonance at frequency of 10.62 THz is due to resonance at these points.

As mentioned in the previous sections, the chemical potential of graphene can be adjusted by electric gating and chemical doping, which is done with an external DC-bias voltage and an electrode layer, as shown in Fig. 11. The electrode layer is usually made of polysilicon and is placed at a very small distance from the graphene, and the thickness of this layer is considered as small as possible so as not to interfere with the performance of the absorber. According to Eq. (16), the VG voltage, shown in Fig. 2a, regulates the chemical potential of graphene (μ_c) (Hanson 2008).

$$V_G = \frac{n_s e T}{\varepsilon_0 \varepsilon_r} \tag{15}$$

where T is the thickness of the dielectric layer between the graphene layer and the electrode layer, ε_r is the relative permittivity of the dielectric, and n_s can be calculated by Eq. (17):

Fig. 11 External DC-bias voltage of graphene
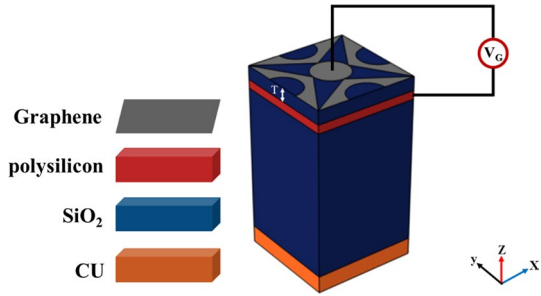
$$n_s = \frac{2}{\pi h^2 V_F^2} \int_0^\infty \varepsilon \left[f_d\left(\varepsilon, \mu_c, T\right) - f_d\left(\varepsilon + 2\mu_c, \mu_c, T\right) \right] d\varepsilon \qquad (16)$$

where $V_F = 9.5 \times 10^5$ m/s is the Fermi velocity, ε represents energy, $f_d\left(\varepsilon, \mu_c, T\right) = \frac{1}{\left(e^{(\varepsilon - \mu_c)/(K_B T)} + 1\right)}$, and $f_d\left(\varepsilon + 2\mu_c, \mu_c, T\right) = \frac{1}{\left(e^{(\varepsilon + \mu_c)/(K_B T)} + 1\right)}$.

It should be noted that when we want to physically implement the regulation of the chemical potential of graphene in such structures, the graphene components with a gap between them must be connected either in series or each must be connected to a separate external DC-bias voltage (With the same voltage VG).

As mentioned, more absorption peaks, high absorption rate, insensitivity to polarization and light incident angle are some of the features that distinguish the metamaterial absorber. For this purpose, in Table 1, we have compared the metamaterial absorber presented in this paper with some of the metamaterial absorbers presented in recent years in terms of having or not having these properties.

As it is known, the proposed absorber has more absorption peaks than some of the compared absorbers (Xing and Jian 2018; Meng et al. 2019; Wang et al. 2020; Li and Cheng 2020; Aksimsek 2020; Rahmanshahi et al. 2021) and has a higher absorption rate than some of them (Appasani et al. 2019; Wang et al. 2020, 2021; Lou et al. 2020; Jiang et al. 2021). In addition, the proposed absorber has the advantage of insensitivity to polarization compared to some of the absorbers (Wang 2017; Xing and Jian 2018; Appasani et al. 2019; Rahmanshahi et al. 2021) presented in Table 1 due to its symmetrical design, and it is also insensitive to the light incident angle at two absorption peaks. As a result, the proposed absorber is more flexible and suitable for many applications such as imaging, detecting, sensing, filtering, etc. due to multi-band absorption, complete absorption, insensitivity to polarization and insensitivity to the light incident angle at its two absorption peaks.

6 Conclusion

In recent years, many terahertz absorbers have been introduced. The absorber presented in this paper is a multi-band perfect metamaterial absorber that has one graphene disk at the center and four graphene solid triangle with semicircular cuts on them that surround the central disk. The proposed absorber is a resonant absorber that has four perfect absorption peaks, which are 99.5%, 99.7%, 94.71% and 97.06% at frequencies of 4.24 THz, 5.89 THz, 9.66 THz, and 10.62 THz, respectively. This structure has the ability to adjust and increase the absorption peaks only by changing the Fermi level or the graphene relaxation time, without the need for structural change. In addition, this absorber is not sensitive

Table 1 Comparison between the features of the absorber structure of different articles with the features of the proposed absorber structure in this paper

Feature Reference	Absorption freq. (THz)/wavelengths (nm)	Absorption peaks	Polarization sensitivity	Light incident angle sensitivity
Wang (2017)	0.60 THz 0.80 THz 1.74 THz 2.33 THz 2.75 THz 3.63 THz	99.10% 99.90% 98.77% 98.82% 99.99% 99.63%	Sensitive to polarization	No analysis has been done
Xing and Jian (2018)	4.95 THz 9.2 THz	99.8% 99.6%	No analysis has been done	No analysis has been done
Appasani et al. (2019)	1.054 THz 2.16 THz 3.59 THz 3.87 THz	90.6% 97.2% 93.95% 99.61%	Sensitive to polarization at three absorption peaks	Insensitive to light incident angle (at a wide angle)
Meng et al. (2019)	0.8 THz 1.72 THz 3.38 THz	99.43% 99.92% 99.58%	Polarization insensitive	Insensitive to light incident angle (at a wide angle) at two absorption peaks
Wang et al. (2020)	0.245 THz	97.5%	Polarization insensitive	Insensitive to light incident angle (at a wide angle)
Li and Cheng (2020)	0.114 THz 0.181 THz	97.9% 99.8%	Polarization insensitive	Insensitive to light incident angle (at a wide angle)
Aksimsek (2020)	1.16 THz 2.73 THz 4.57 THz	99.6% 99.8% 99.5%	Polarization insensitive	Insensitive to light incident angle (at a wide angle) at two absorption peaks

Table 1 (continued)

Feature Reference	Absorption freq. (THz)/wavelengths (nm)	Absorption peaks	Polarization sensitivity	Light incident angle sensitivity
Lou et al. (2020)	0.80 THz 2.89 THz 3.98 THz 4.36 THz	In an average of 97.54%	Polarization insensitive	No analysis has been done
Rahmanshahi et al. (2021)	1.92 THz 4.62 THz 8.81 THz	98.4% 98.3% 99.6%	No analysis has been done	No analysis has been done
Wang et al. (2021)	2.59 THz (OS) 3.03 THz (OS) 6.54–7.10 THz (OS) 3.12 THz (TS) 6.00–7.21 THz (TS)	Larger than 90%	Polarization insensitive in both TS and OS	Sensitive to light incident angle in both TS and OS
Jiang et al. (2021)	1085.03 nm 1131.48 nm 1187 nm 1365.35 nm	95.88% 99.81% 97.44% 95.30%	Insensitive to polarization in TM mode	Insensitive to light incident angle (at a wide angle) in TM mode
Proposed absorber	4.24 THz 5.89 THz 9.66 THz 10.62 THz	99.5% 99.7% 94.71% 97.06%	Polarization insensitive	Insensitive to light incident angle at two absorption peaks and high tolerance to light incident angle at other absorption peaks (at a wide angle)

to polarization due to its symmetrical design and its two absorption peaks remain almost unchanged in various light incident angles (from 0 to 45 degrees). All these features make the absorber very suitable for applications such as imaging, detection, sensing and filtering.

Data availability   All data generated or analyzed during this study are included in this published article.

Declarations

Conflict of interest   The authors declare that they have no known competing financial interests or personal relationships that could have appeared to influence the work reported in this paper.

References

Aksimsek, S.: Design of an ultra-thin, multiband, micro-slot based terahertz metamaterial absorber. Electromag. Wav. Appl. **34**(16), 2181–2193 (2020)

Appasani, B., Prince, P., Ranjan, R.K., Gupta, N., Verma, V.K.: A simple multi-band metamaterial absorber with combined polarization sensitive and polarization insensitive characteristics for terahertz applications. Plasmonics **14**, 737–742 (2019)

Bağmancı, M., Karaaslan, M., Ünal, E., et al.: Extremely-broad band metamaterial absorber for solar energy harvesting based on star shaped resonator. Opt. Quant. Electron. **49**, 257 (2017)

Bai, J., Shen, W., Shi, J., Xu, W., Zhang, S., Chang, S.: A non-volatile tunable terahertz metamaterial absorber using graphene floating gate. Micromachines **12**(3), 333 (2021)

Barzegar-Parizi, S.: Graphene-based tunable dual-band absorbers by ribbon/disk array. Opt. Quant. Electron. **51**, 1–11 (2019)

Barzegar-Parizi, S., Rejaei, B., Khavasi, A.: Analytical circuit model for periodic arrays of graphene disks. IEEE J. Quant. Electron. **51**(9), 1–7 (2015)

Bendelala, F., Cheknane, A., Hilal, H.S.: A broad-band polarization-insensitive absorber with a wide angle range metamaterial for thermo-photovoltaic conversion. Opt. Quant. Electron. **50**, 1–10 (2018)

Cai, W., Chettiar, U.K., Kildishev, A.V., Shalaev, V.M.: Optical cloaking with metamaterials. Nat. Photonics **1**, 224–227 (2007)

Chahkoutahi, A., Emami, F.: Design of novel sensitive terahertz metamaterial absorbers based on graphene-plasmonic nanostructures. Opt. Quant. Electron. **53**, 1–14 (2021)

Chen, P.Y., Alù, A.: Atomically thin surface cloak using graphene monolayers. ACS Nano **5**(7), 5855–5863 (2011)

Deljoo, H., Rostami, A.: Broadband terahertz absorber using superimposed graphene quantum dots. Opt. Quant. Electron. **53**, 1–17 (2021)

Deng, X.H., Liu, J.T., Yuan, J., Wang, T.B., Liu, N.H.: Tunable THz absorption in graphene-based heterostructures. Opt. Express **22**(24), 30177–30183 (2014)

Deng, Y., Cao, G., Wu, Y., Zhou, X., Liao, W.: Theoretical description of dynamic transmission characteristics in MDM waveguide aperture-side-coupled with ring cavity. Plasmonics **10**, 1537–1543 (2015)

Deng, Y., Cao, G., Yang, H., Zhou, X., Wu, Y.: Dynamic control of double plasmon-induced transparencies in aperture-coupled waveguide-cavity system. Plasmonics **13**, 345–352 (2018)

Elrashidi, A., Tharwat, M.M.: Broadband absorber using ultra-thin plasmonic metamaterials nanostructure in the visible and near-infrared regions. Opt. Quant. Electron. **53**, 1–11 (2021)

Feng, S., Zhao, Y., Liao, Y.L.: Dual-band dielectric metamaterial absorber and sensing applications. Results Phys. **18**, 103272 (2020)

Fu, Y., Li, S., Chen, Y., et al.: A multi-band absorber based on a dual-trident structure for sensing application. Opt. Quant. Electron. **53**, 1–11 (2021)

Ghods, M.M., Rezaei, P.: Graphene-based Fabry-Perot resonator for chemical sensing applications at mid-infrared frequencies. IEEE Photon Technol. Lett. **30**(22), 1917–1920 (2018a)

Ghods, M.M., Rezaei, P.: Ultra-wideband microwave absorber based on uncharged graphene layers. J. Electromag. Wav. Appl. **32**(15), 1950–1960 (2018b)

Gong, J., Shi, X., Lu, Y., Hu, F., Zong, R., Li, G.: Dynamically tunable triple-band terahertz perfect absorber based on graphene metasurface. Superlattice. Microst. **150**, 106797 (2021)

Hanson, G.W.: Dyadic green's functions for an anisotropic, non-local model of biased graphene. IEEE Trans. Antennas Propag. **56**(3), 747–757 (2008)

Jafari-Chashmi, M., Rezaei, P., Kiani, N.: Reconfigurable graphene-based V-shaped dipole antenna: from quasi-isotropic to directional radiation pattern. Optik **184**, 421–427 (2019)

Jafari-Chashmi, M., Rezaei, P., Kiani, N.: Polarization controlling of multi resonant graphene-based microstrip antenna. Plasmonics **15**, 417–426 (2020a)

Jafari-Chashmi, M., Rezaei, P., Kiani, N.: Y-shaped graphene-based antenna with switchable circular polarization. Optik **200**, 163321 (2020b)

Jiang, L., Yuan, C., Li, Z., Su, J., Yi, Z., Yao, W., Wu, P., Liu, Z., Cheng, S., Pan, M.: Multi-band and high-sensitivity perfect absorber based on monolayer graphene metamaterial. Diam. Relat. Mater. **111**, 108227 (2021)

Katsnelson, M.I.: Graphene: carbon in two dimensions. Mater. Today **10**(1), 20–27 (2007)

Ke, R., Liu, W., Tian, J., Yang, R., Pei, W.: Dual-band tunable perfect absorber based on monolayer graphene pattern. Result. Phys. **18**, 103306 (2020)

Kiani, N., Tavakkol-Hamedani, F., Rezaei, P.: Polarization controlling idea in graphene-based patch antenna. Optik **239**, 166795 (2021a)

Kiani, S., Rezaei, P., Fakhr, M.: An overview of interdigitated microwave resonance sensors for liquid samples permittivity detection, in Interdigital sensors: Progress over the last two decades. Springer **7**, 153–197 (2021b)

Kshetrimayum, R.S.: A brief intro to metamaterials. IEEE Potentials **23**(5), 44–46 (2004)

Li, W., Cheng, Y.: Dual-band tunable terahertz perfect metamaterial absorber based on strontium titanate (STO) resonator structure. Opt. Commun. **462**, 125265 (2020)

Li, Q., Gao, J., Yang, H., et al.: Mechanism investigation of a narrow-band super absorber using an asymmetric Fabry-Perot cavity. Opt. Quant. Electron. **49**, 159 (2017)

Lou, P., Wang, B.X., He, Y., et al.: Simplified design of quad-band terahertz absorber based on periodic closed-ring resonator. Plasmonics **15**, 1645–1651 (2020)

Meng, T., Hu, D., Zhu, Q.: Design of a five-band terahertz perfect metamaterial absorber using two resonators. Opt. Commun. **415**, 151–155 (2018)

Meng, W., Que, L., Lv, J., Zhang, L., Zhou, Y., Jiang, Y.: A triple-band terahertz metamaterial absorber based on buck Dirac semimetals. Results Phys. **14**, 102461 (2019)

Ni, B., Wang, Z.Y., Zhao, R.S., et al.: Realisation of a humidity sensor based on perfect metamaterial absorber. Opt. Quant. Electron. **49**, 1–7 (2017)

Norouzi-Razani, A., Rezaei, P.: Broadband polarization insensitive and tunable terahertz metamaterial perfect absorber based on the graphene disk and square ribbon. Superlattice. Microst. **63**, 107153 (2022)

Pan, M., Huang, H., Fan, B., Chen, W., Li, S., Xie, Q., Xu, F., Wei, D., Fang, J.: Theoretical design of a triple-band perfect metamaterial absorber based on graphene with wide-angle insensitivity. Result. Phys. **23**, 104037 (2021)

Pendry, J.B.: Negative refraction makes a perfect lens. Phys. Rev. Lett. **85**(18), 3966–3969 (2000)

Perruisseau-Carrier, J.: Graphene for antenna applications: Opportunities and challenges from microwaves to THz. Loughborough Antennas Propag. Conf. (LAPC) UK 1–4 (2012)

Pop, E., Varshney, V., Roy, A.K.: Thermal properties of graphene: Fundamentals and applications. MRS Bull. **37**(12), 1273–1281 (2012)

Rahmanshahi, M., Noori-Kourani, S., Golmohammadi, S., Baghban, H., Vahed, H.: A tunable perfect THz metamaterial absorber with three absorption peaks based on nonstructured graphene. Plasmonics **16**, 1665–1676 (2021)

Rezagholizadeh, E., Biabanifard, M., Borzooei, S.: Analytical design of tunable THz refractive index sensor for TE and TM modes using graphene disks. J. Phys.: Appl. Phys. **53**(29), 295107 (2020)

Shalini, V.B.: A polarization insensitive miniaturized pentaband metamaterial THz absorber for material sensing applications. Opt. Quant. Electron. **53**, 1–14 (2021)

Shin, D., Urzhumov, Y., Jung, Y., Kang, G., Baek, S., Choi, M., Park, H., Kim, K., Smith, D.R.: Broadband electromagnetic cloaking with smart metamaterials. Nat. Commun. **3**(1213), 1–8 (2012)

Simovski, C.R., Belov, P.A., He, S.L.: Backward wave region and negative material parameters of a structure formed by lattices of wires and split-ring resonators. IEEE Trans. Antennas Propag. **51**(10), 2582–2591 (2003)

Smith, D.R., Pendry, J.B., Wiltshire, M.C.K.: Metamaterials and negative refractive index. Science **305**(5685), 788–792 (2004)

Song, W., Teng, Y., Zhang, Z.Q., Li, J.W., Sun, J., Chen, C.H., Zhang, L.J.: Rapid startup in relativistic backward wave oscillator by injecting external backward signal. Phys. Plasmas **19**(8), 1–4 (2012)

Song, Z., Wang, K., Li, J., Liu, Q.H.: Broadband tunable terahertz absorber based on vanadium dioxide metamaterials. Opt. Express **26**(6), 7148–7154 (2018)

Tahseen, M.M., Kishk, A.A.: Wideband textile-based conformal antennas for WLAN band using conductive thread. In: 10th Europ Conf Antennas Propag, Davos, Switzerland, pp. 1–5 (2016)

Valentine, J., Zhang, S., Zentgraf, T., Ulin-Avila, E., Genov, D.A., Bartal, G., Zhang, X.: Three-dimensional optical metamaterial with a negative refractive index. Nature **455**, 376–379 (2008)

Veselago, V.G.: The electrodynamics of substances with simultaneously negative values of ε and μ. Sov. Phys. Uspekhi **10**(4), 509–514 (1968)

Wang, B.X., Wang, G.Z., Sang, T., Wang, L.L.: Six-band terahertz metamaterial absorber based on the combination of multiple-order responses of metallic patches in a dual-layer stacked resonance structure. Sci. Rep. **7**, 1–9 (2017)

Wang, J., Lang, T., Hong, Z., Shen, T., Wang, G.: Tunable terahertz metamaterial absorber based on electricity and light modulation modes. Opt. Mater. Express **10**(9), 2262–2273 (2020)

Wang, Z.L., Hu, C.X., Liu, H.B., Zhang, H.F.: A newfangled terahertz absorber tuned temper by temperature field doped by the liquid metal. Plasmonics **16**, 425–434 (2021)

Wu, J.: Tunable multi-band terahertz absorber based on graphene nano-ribbon metamaterial. Phys. Lett. A **383**(22), 2589–2593 (2019)

Wu, X., Zheng, Y., Luo, Y., Zhang, J., Yi, Z., Wu, X., Cheng, S., Yang, W., Yu, Y., Wu, P.: A four-band and polarization-independent BDS-based tunable absorber with high refractive index sensitivity. Phys. Chem. Chem. Phys. **23**(47), 26864–26873 (2021)

Xiao, B., Lin, H., Xiao, L., et al.: A tunable dual-band THz absorber based on graphene sheet and ribbons. Opt. Quant. Electron. **50**, 1–8 (2018)

Xing, R., Jian, S.: A dual-band THz absorber based on graphene sheet and ribbons. Opt. Laser Technol. **100**, 129–132 (2018)

Yao, G., Ling, F., Yue, J., Luo, C., Ji, J., Yao, J.: Dual-band tunable perfect metamaterial absorber in the THz range. Opt. Express **24**(2), 1518–1527 (2016)

Yi, Z., Lin, H., Niu, G., Chen, X., Zhou, Z., Ye, X., Duan, T., Yi, Y., Tang, Y., Yi, Y.: Graphene-based tunable triple-band plasmonic perfect metamaterial absorber with good angle-polarization-tolerance. Result. Phys. **13**, 102149 (2019)

Zamzam, P., Rezaei, P.: A terahertz dual-band metamaterial perfect absorber based on metal-dielectric-metal multi-layer columns. Opt. Quant. Electron. **53**, 1–9 (2021)

Zamzam, P., Rezaei, P., Khatami, S.A.: Quad-band polarization-insensitive metamaterial perfect absorber based on bilayer graphene metasurface. Phys. E: Low-Dimens. Syst. Nanost. **128**, 114621 (2021)

Zhang, J., Tian, J., Li, L.: A dual-band tunable metamaterial near-unity absorber composed of periodic cross and disk graphene arrays. IEEE Photon. J. **10**(2), 1–12 (2018)

Zhao, F., Lin, J., Lei, Z., Yi, Z., Qin, F., Zhang, J., Liu, L., Wu, X., Yang, W., Wu, P.: Realization of 18.97% theoretical efficiency of 0.9 µm thick c-Si/ZnO heterojunction ultrathin-film solar cells via surface plasmon resonance enhancement. Phys. Chem. Chem. Phys. **24**(8), 4871–4880 (2022)

Zheng, Z., Zheng, Y., Luo, Y., Yi, Z., Zhang, J., Liu, Z., Yang, W., Yu, Y., Wu, X., Wu, P.: A switchable terahertz device combining ultra-wideband absorption and ultra-wideband complete reflection. Phys. Chem. Chem. Phys. **24**(4), 2527–2533 (2022)

Zhou, F., Qin, F., Yi, Z., Yao, W., Liu, Z., Wu, X., Wu, P.: Ultra-wideband and wide-angle perfect solar energy absorber based on Ti nanorings surface plasmon resonance. Phys. Chem. Chem. Phys. **23**(31), 17041–17048 (2021)